Theoretical description of Shack–Hartmann wave-front sensor

Jérôme Primot*

*Office National d'Etudes et de Recherches Aérospatiales, Département d'Optique Théorique et Appliquée,
Chemin de la Hunière, 91 761 Palaiseau, Cedex, France*

Abstract

In this paper, we propose a complete model of Shack–Hartmann wave-front sensor, seen as a grating interferometer. A new technique for extracting the phase derivative is also proposed and the exact quantity measured is detailed.
© 2003 Elsevier Science B.V. All rights reserved.

1. Introduction

The Shack–Hartmann wave-front sensor (SHWFS) is a very common device, especially in the field of adaptive optics [1], but is nonetheless poorly known in the field of interferometry. Indeed, to our knowledge, no paper has been completely devoted to its theory [2]. This is probably due to two facts. First, the birth of this system is only related in an abstract of one of Shack's conferences [3]. Second, its operation appeals to the intuition, which gives the overall impression that the underlying theory is obvious. However, when considering the way the complex grid of microlenses constituting the main component of the SHWFS acts upon the analyzed wave-front, the mode of operation is not so easy to describe.

The purpose of this paper is to present a theoretical model of SHWFS, seen as a grating interferometer, as presented in Section 2. Section 3 models the irradiance pattern obtained in the common focal plane of microlenses (called Hartmanngram hereafter). Two domains, are distinguished, considering the strength of the crosstalk between lenslets. Then, Section 4 describes the extraction of phase derivatives. To conclude, the quantity actually measured by SHWFS is summarized.

---

* Tel.: +33-169936386; fax: +33-169936345.
  E-mail address: jerome.primot@onera.fr.

2. SHWFS description

The original description of SHWFS by Shack and Platt is based on the following model [4]. The analyzed wave-front is sampled by a microlens array, leading to almost plane sub-wave-fronts, as shown in Fig. 1.

The focal spot at the focus of each lenslet is then translated laterally, proportional to the slope of the associated sub-wave-front. In this model, the assumption is that each lenslet is independent of consecutive lenslets. So, it is limited to microlens arrays with low F-number.

Here, we propose to consider that the microlens array is a phase grating, following the remark made by Roddier [5]. So, SHWFS can be seen as a grating interferometer.

The expression of the phase grating is equal to $G(x,y)$

$$G(x,y) = \left[\exp\left(i\pi \frac{(x^2 + y^2)}{\lambda f_{\mu l}} \right) \Pi_{p,p}(x,y) \right] * \mathrm{comb}_{p,p}(x,y) \tag{1}$$

with

$$\begin{cases} \Pi_{p,p}(x,y) = 1, & \text{for} -p/2 < x < p/2, \ -p/2 < y < p/2 \\ \Pi_{p,p}(x,y) = 0, & \text{elsewhere} \end{cases}$$

and p is the microlens pitch, $f_{\mu l}$ is the focal length of lenslets, λ is the wavelength, $\mathrm{comb}_{p,p}(x,y)$ is the bi-directional Dirac comb function of p pitch and * is the convolution product.

As $G(x,y)$ is a bi-periodic function, it can be expressed as

$$G(x,y) = \frac{1}{p^2} \sum_{n=-\infty}^{+\infty} \sum_{m=-\infty}^{+\infty} c_{n,m} \exp\left(\frac{2i\pi}{p}(nx + my) \right) \tag{2}$$

with

$$c_{n,m} = \int_{-\infty}^{\infty} \int_{-\infty}^{\infty} \Pi_{p,p}(x,y) \exp\left(i\pi \frac{(x^2 + y^2)}{\lambda f_{\mu l}} \right) \exp\left(-\frac{2i\pi}{p}(nx + my) \right) dx\,dy \tag{3}$$

or

$$c_{n,m} = \mathrm{FT}\left[\Pi_{p,p}(x,y) \exp\left(i\pi \frac{(x^2 + y^2)}{\lambda f_{\mu l}} \right) \right]_{n/p,m/p} \tag{4}$$

with FT, the Fourier transform of the function under brackets at the point $(n/p, m/p)$.
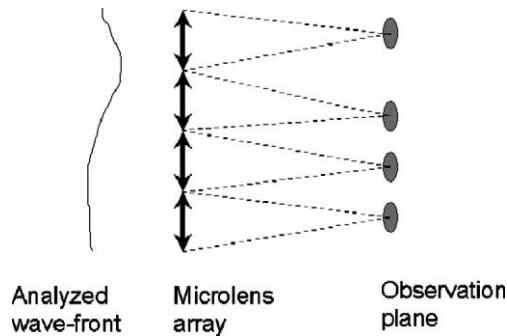

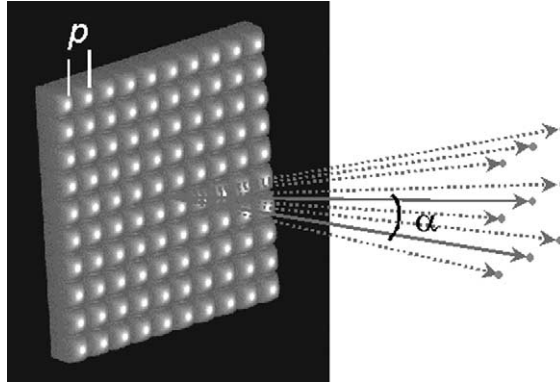Fig. 1. Classical description of Shack–Hartmann wave-front sensor.

Fig. 2. Microlens array seen as a two-dimensional phase grating, with diffracted orders.

So, Eq. (4) can be re-expressed as

$$c_{n,m} = \Psi_{\mu l}\left(\frac{n}{p}, \frac{m}{p}\right) \tag{5}$$

with

$$\Psi_{\mu l}(u,v) = \left(\frac{\sin(\pi p u)}{\pi p u} \frac{\sin(\pi p v)}{\pi p v}\right) * \exp\left(i\pi\lambda f_{\mu l}(u^2 + v^2)\right). \tag{6}$$

If the square grating $G(x, y)$ is illuminated by a monochromatic almost plane wave, parallel to its plane, replicas of the wave are diffracted. All of them have an angular deviation, as described in Fig. 2.

Assuming that the pitch p is large with respect to the wavelength, and that analyzed wave-front is small with respect to the amplitude of the phase grating, the irradiance pattern can be seen as the interference of wave-front replicas, each of them being tilted with a wave-vector equal to $\mathbf{k}_{n,m}$

$$\mathbf{k}_{n,m} = \frac{2\pi}{\lambda}\left(n\alpha, m\alpha, \sqrt{1 - (n^2 + m^2)\alpha^2}\right) \tag{7}$$

with α being equal to

$$\alpha = \frac{\lambda}{p}. \tag{8}$$

Considering Eq. (6), it is not easy to compute $c_{n,m}$ values. However, it has to be noticed that this expression is analogous to the expression of the amplitude at the $(n\lambda, m\lambda)$ point of the focal plane of a F/1 square lens of size p, for the observation of a point source P placed at a $f_{\mu l}$ distance. This analogy is illustrated in Fig. 3.

Considering the relative rates of variation of the functions convolved in Eq. (5), we find two domains. The first one is called ''independence domain''; it corresponds to lenslets having a low F-number. In this case, no crosstalk has to be considered between consecutive lenslets. So, the second domain is called ''crosstalk domain''.

2.1. Independence domain

Taking into account the analogy presented in Fig. 3, we see that Eq. (5) can be simplified when $f_{\mu l}$ is not too high with respect to p (lenslets of low F-number). Indeed, the point source P is strongly defocused, and geometrical approximation applies, so Eq. (5) reduces to
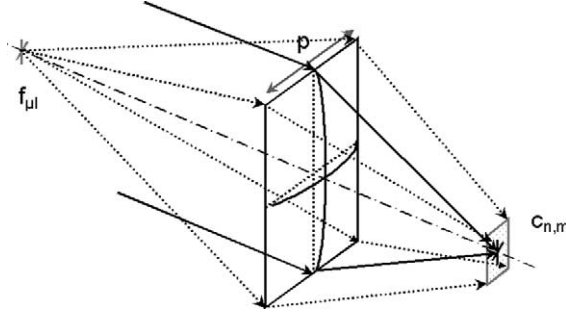
Fig. 3. Illustration of the analogy. $C_{n,m}$ are equal to the values of the amplitude obtained at $(n\lambda, m\lambda)$ point of the focal plane for a F/1 square lens of focal length p, considering a defocalized point P placed at $f_{\mu l}$.

$$\begin{cases} c_{n,m} = \exp\left(i\pi \frac{\lambda f_{\mu l}}{p^2}\right), (|c_{n,m}| = 1), & \text{for} -H < n < H, \ -H < m < H \\ c_{n,m} = 0, & \text{elsewhere} \end{cases} \tag{9}$$

with

$$H = \text{int}\left(\frac{p^2}{2\lambda f_{\mu l}}\right), \tag{10}$$

where int is the integer part of the expression under brackets.

Consider now the amplitude $A(x, y, L)$ observed in a plane distant of L, when the grating is illuminated by a plane wave-front

$$A(x, y, L) = G(x, y) * F(x, y, L), \tag{11}$$

where $F(x, y, L)$ is the Fresnel operator

$$F(x, y, L) = \exp\left(-\frac{i\pi}{\lambda L}(x^2 + y^2)\right). \tag{12}$$

Considering Eqs. (11) and (5), the Fourier transform of A, $\text{FTA}(u, v, L)$, is then equal to

$$\text{FTA}(u, v, L) = \sum_{n=-H}^{H} \sum_{m=-H}^{H} c_{n,m} \exp\left(-\frac{i\pi\lambda L}{p^2}(n^2 + m^2)\right) \delta\left(u - \frac{n}{p}, v - \frac{m}{p}\right) \tag{13}$$

with $\delta(u, v)$, the Dirac function.

In the focal plane of microlenses, L is equal to $f_{\mu l}$, and Eq. (13) reduces to

$$\text{FTA}(u, v, f_{\mu l}) = \sum_{n=-H}^{H} \sum_{m=-H}^{H} \delta\left(u - \frac{n}{p}, v - \frac{m}{p}\right), \tag{14}$$

and

$$A(x, y, f_{\mu l}) = \sum_{n=-H}^{H} \sum_{m=-H}^{H} \exp\left(\frac{2i\pi}{p}(nx + my)\right). \tag{15}$$

Thus, for microlens arrays with low F-number, the recorded Hartmanngram can be described as the interference of $(2H + 1)$ by $(2H + 1)$ tilted replicas of equal amplitude of the analyzed wave-front.

Notice that H corresponds to the integer part of κ, ratio between the pitch p and the width of the spot $2\lambda f_{\mu l}/p$ observed at the focal plane of an independent lenslet; so, κ can be defined as a compression ratio.

In this case, the extremities of the wave vectors of the replicas define a square, corresponding to the contributing part of the analyzed wave-front. The size of this square is equal to C_G

$$C_{G} = (2H + 1)\alpha f_{\mu l}. \tag{16}$$

Taking into account Eqs. (8) and (10), and considering that H is large, C reduces to

$$C_{G} \cong p. \tag{17}$$

So, for an array of low F-number microlenses, the assumption of independent lenslets is globally verified, as the contributions of the analyzed wave-front are all coming from a surface corresponding to the support of a lenslet. The classical model proposed by Platt and Shack [4] is then verified.

2.2. Limits of the independence domain

The model described here-before is very simple and of great interest for understanding how the SHWFS operates. Unfortunately, the independence assumption is not relevant in most applications found in the literature.

For example, Fig. 4 shows the modulus of the $c_{n,0}$ for H equal to 4, i.e., a focal spot a quarter of a sub-aperture wide. It can be seen that the number of orders of non-negligible amplitudes is greater than H by a factor of 2, if we take 10% of the largest amplitude as a limit. In fact, the independence assumption applies only when H exceeds 20. However, for most applications, H is comprised in between 2 and 6, with a privileged value of 4. That is, the constraints of high bandpass and low light level for controlling an adaptive optics requires the use of a sensor with a low number of pixels, and thus a low compression ratio.

Therefore, in these cases, the number of diffracted orders H_{NG} exceeds H, and the amplitude $A_{NG}(x, y, f_{\mu l})$ is expressed as

$$A_{NG}(x, y, f_{\mu l}) = \sum_{n=-H_{NG}}^{H_{NG}} \sum_{m=-H_{NG}}^{H_{NG}} c_{n,m} \exp\left(\frac{-i\pi\lambda f_{\mu l}}{p^2}(n^2 + m^2)\right) \exp\left(\frac{2i\pi}{p}(nx + my)\right). \tag{18}$$
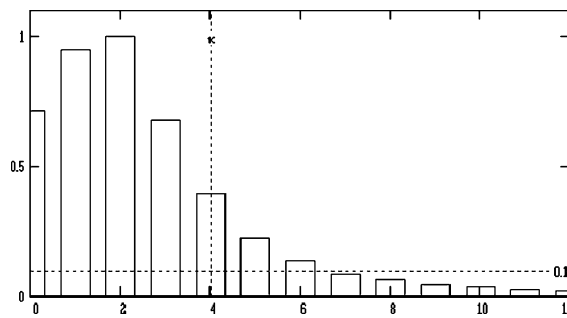

Fig. 4. Amplitudes of $c_{n,0}$, for a compression ratio of 4.

Table 1
Evaluation of H_{NG} and C_{NG} for different values of H

H	H_{NG}	$C_{NG} \times p$
2	4	2.5
4	7	2
6	10	1.8
10	15	1.6
20	27	1.4
50	62	1.2

C_{NG}, expressed in multiple of p, corresponds to the size of the surface of the analyzed wave-front from which significant contributions are issued.

Thus, for microlens array with high F-number, the Hartmanngram can be described as the interference of $2H_{NG} + 1$ by $2H_{NG} + 1$ replicas of unequal amplitudes of the analyzed wave-front. Now, C_{NG}, the size of the square defined by the extremities of the wave vectors, is strictly greater than p.

Table 1 gives C_{NG} for different values of H, if H_{NG} is limited to the orders having an amplitude higher than 10% of the highest order. It can be seen that the assumption of independent lenslets is no longer valid because significant contributions come from an area much larger than a sub-aperture.

3. The Hartmanngram

As described above, assuming that the analyzed wave-front variations are small with respect to the microlens grid, SHWFS can be seen as a lateral shearing interferometer, based on the interference of replicas of various amplitudes, each tilted in x- and y-directions. So, in the general case, for a wave-front uniform in intensity, the amplitude in the focal plane is equal to $A_{ANA}(x, y)$

$$A_{ANA}(x,y) = \sum_{n=-H_t}^{H_t} \sum_{m=-H_t}^{H_t} c_{n,m} \exp\left(\frac{-i\pi}{2H}(n^2 + m^2)\right) \exp\left(i\Phi\left(x + \frac{np}{2H}, y + \frac{mp}{2H}\right)\right)$$
$$\times \text{Support}\left(x + \frac{np}{2H}, y + \frac{mp}{2H}\right) \exp\left(\frac{2i\pi}{p}(nx + my)\right) \tag{19}$$

with H_t equal to H or H_{NG}, and $\text{Support}(x, y)$, the support of the analyzed pupil.

For the sake of simplicity, we will consider here that the support is large, i.e., the SHWFS has a large number of sub-apertures. In this case, A_{ANA} can be approximated by

$$A_{ANA}(x,y) = \sum_{n=-H_{NG}}^{H_{NG}} \sum_{m=-H_{NG}}^{H_{NG}} c_{n,m} \exp\left(\frac{-i\pi}{2H}(n^2 + m^2)\right) \exp\left(i\Phi\left(x + \frac{np}{2H}, y + \frac{mp}{2H}\right)\right) \exp\left(\frac{2i\pi}{p}(nx + my)\right). \tag{20}$$

We can now evaluate the intensity in the common focal plane, for the two domains.

3.1. Independence domain

We will first consider this case because, while shown to be irrelevant, it corresponds to the classical description of the SHWFS. The irradiance pattern $I_G(x, y)$ is equal to:

$$I_G(x,y) = \sum_{n,m=-H}^{H} \sum_{n',m'=-H}^{H} \exp\left(i\left(\Phi\left(x + \frac{np}{2H}, y + \frac{mp}{2H}\right) - \Phi\left(x + \frac{n'p}{2H}, y + \frac{m'p}{2H}\right)\right)\right)$$
$$\times \exp\left(\frac{2i\pi}{p}\left((n - n')x + (m - m')y\right)\right). \tag{21}$$

Assuming that the analyzed wave-front is well sampled, i.e., that its variations are small at the scale of a sub-aperture, we can consider that

$$\Phi\left(x + \frac{np}{2H}, y + \frac{mp}{2H}\right) = \Phi(x, y) + \frac{np}{2H}\frac{\partial \Phi}{\partial x}(x, y) + \frac{mp}{2H}\frac{\partial \Phi}{\partial y}(x, y). \tag{22}$$

So, from Eqs. (21) and (22), with $k = n - n'$ and $l = m - m'$

$$I_G(x,y) = \sum_{k=-2H}^{2H} \sum_{l=-2H}^{2H} \text{Harm}_{k,l}(x, y) \exp\left(\frac{2i\pi}{p}(kx + ly)\right) \tag{23}$$

with

$$\text{Harm}_{k,l}(x,y) = (2H + 1 - |k|)(2H + 1 - |l|) \exp\left(i\frac{p}{2H}\left(k\frac{\partial \Phi}{\partial x}(x,y) + l\frac{\partial \Phi}{\partial y}(x,y)\right)\right). \tag{24}$$

So, $\text{FTI}_G(u,v)$, Fourier transform of the irradiance pattern, is equal to

$$\text{FTI}_G(u,v) = \sum_{k=-2H}^{2H} \sum_{l=-2H}^{2H} \text{FTHarm}_{k,l}(u,v) * \delta\left(u - \frac{k}{p}, v - \frac{l}{p}\right) \tag{25}$$

with $\text{FTHarm}_{k,l}(u,v)$, the Fourier transform of $\text{Harm}_{k,l}(x,y)$. The spectrum of I_G consists of $(4H + 1)^2$ harmonics $\text{FTHarm}_{k,l}(u,v)$ placed on a square grid of pitch $1/p$ with decreasing amplitudes.

However, the assumption made here is very restrictive, especially for the first harmonics. Consider, for example, $\text{Harm}_{1,0}(x,y)$

$$\text{Harm}_{1,0}(x,y) = \sum_{n=-H}^{H-1} \sum_{m=-H}^{H} \exp\left(i\left(\Phi\left(x + \frac{np}{2H}, y + \frac{mp}{2H}\right) - \Phi\left(x + \frac{(n+1)p}{2H}, y + \frac{mp}{2H}\right)\right)\right). \tag{26}$$

Assuming that the variation of Φ is small on the scale of p/H (and not on the scale of p), $\text{Harm}_{1,0}$ can be approximated by

$$\text{Harm}_{1,0}(x,y) = \sum_{n=-H}^{H-1} \sum_{m=-H}^{H} 1 + i\left[\Phi\left(x + \frac{np}{2H}, y + \frac{mp}{2H}\right) - \Phi\left(x + \frac{(n+1)p}{2H}, y + \frac{mp}{2H}\right)\right], \tag{27}$$

so

$$\text{Harm}_{1,0}(x,y) = 2H(2H + 1) + i\sum_{m=-H}^{H} \Phi\left(x - \frac{p}{2}, y + \frac{mp}{2H}\right) - \Phi\left(x + \frac{p}{2}, y + \frac{mp}{2H}\right). \tag{28}$$

As H is large, we find that the imaginary part of $\text{Harm}_{1,0}(x,y)$ is proportional to the difference of the mean phase on the two opposite sides of a sub-aperture

$$\text{Im}(\text{Harm}_{1,0}(x,y)) \propto \int_{-p/2}^{p/2} \Phi\left(x - \frac{p}{2}, y\right) - \Phi\left(x + \frac{p}{2}, y\right) dy. \tag{29}$$

The same result is obtained for $\text{Harm}_{k,l}(x,y)$, assuming that the phase variations are small on the scale of $\eta_{k,l}$

$$\eta_{k,l} = \left(\frac{kp}{H}, \frac{lp}{H}\right). \tag{30}$$

It should be noted that the imaginary part of the first harmonic is equal to the quantity deduced from the geometrical model, taking into account the centroiding step [6].

3.2. Crosstalk domain

$I_{\text{NG}}(x,y)$, the irradiance pattern observed in the focal plane of microlenses in the general case, is expressed as

$$I_{\text{NG}}(x,y) = \sum_{n,m=-H_{\text{NG}}}^{H_{\text{NG}}} \sum_{n',m'=-H_{\text{NG}}}^{H_{\text{NG}}} \gamma_{n,m} \gamma_{n',m'}^* \exp\left(i\left(\Phi\left(x + \frac{np}{2H}, y + \frac{mp}{2H}\right) - \Phi\left(x + \frac{n'p}{2H}, y + \frac{m'p}{2H}\right)\right)\right)$$
$$\times \exp\left(\frac{2i\pi}{p}\left((n - n')x + (m - m')y\right)\right) \tag{31}$$

with

$$\gamma_{n,m} = \Psi_{\mu l}\left(\frac{n}{p},\frac{m}{p}\right)\exp\left(\frac{-i\pi}{2H}(n^2+m^2)\right), \tag{32}$$

and $\gamma_{n,m}^*$, the conjugated complex of $\gamma_{n,m}$.

Consider first that the analyzed wave-front varies slowly on the scale of p_{NG}

$$p_{NG} = \frac{H_{NG}}{H}p. \tag{33}$$

The result is then similar to that of Section 3.1

$$I_{NG}(x,y) = \sum_{k=-H_{NG}}^{H_{NG}}\sum_{l=-H_{NG}}^{H_{NG}} \mathrm{Harm}_{k,l}^{NG}(x,y)\exp\left(\frac{2i\pi}{p}(kx+ly)\right) \tag{34}$$

with

$$\mathrm{Harm}_{k,l}^{NG}(x,y) = \Gamma_{\mu l}\left(\frac{k}{p},\frac{l}{p}\right)\exp\left(i\frac{p}{2H}\left(k\frac{\partial\Phi}{\partial x}(x,y)+l\frac{\partial\Phi}{\partial y}(x,y)\right)\right), \tag{35}$$

and

$$\Gamma_{\mu l}(u,v) = \left(\Psi_{\mu l}(u,v)\exp\left(\frac{-i\pi}{2H}(u^2+v^2)\right)\right) \otimes \left(\Psi_{\mu l}(u,v)\exp\left(\frac{-i\pi}{2H}(u^2+v^2)\right)\right), \tag{36}$$

where $\otimes$ denotes the auto-correlation.

However, the approximation made is now very restricting. For example, for H equal to 4, phase variations are assumed to be small on the scale of twice the sub-aperture size.

If we consider now the only first harmonics, with the same assumption as in Section 3.1 that the phase variations are small on the scale of p/H, we find

$$\mathrm{Im}\left(\mathrm{Harm}_{1,0}^{NG}(x,y)\right) = \sum_{n=-H_{NG}}^{H_{NG}-1}\sum_{m=-H_{NG}}^{H_{NG}} \frac{p}{2H}\mathrm{Re}\left(\gamma_{n,m}\gamma_{n+1,m}^*\right)\frac{\partial\Phi}{\partial x}\left(x+\frac{np}{2H},y+\frac{mp}{2H}\right). \tag{37}$$

Compared to the previous case of independence assumption, we now have a weighted sum of consecutive local phase derivatives. As H_{NG} is now relatively small, the integral form proposed in Eq. (29) is no more possible. Notice also that, as H_{NG} is strictly greater than H (a factor 2 for H equal to 4), this weighted sum involves phase derivatives coming from a much larger surface than the surface of a sub-aperture. However, due to the decrease in amplitude of diffracted orders, weights are significant only for the first orders. Fig. 5
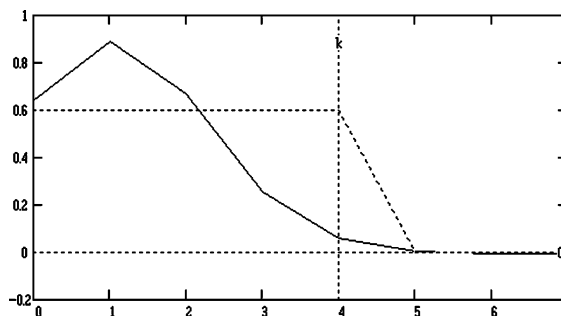

Fig. 5. Weighting function of the phase derivative for the first harmonic $\mathrm{Harm}_{1,0}(x,y)$, for κ equal to 4. The dotted curve corresponds to the approximation of independent lenslets.

shows a cut of the weighting function in the *x*-direction, compared to the geometrical approximation, for *H* equal to 4.

3.3. Recorded Hartmanngram

We have not considered the detection of the Hartmanngram so far. However, it is a fundamental step, as the pixel size is relatively large with respect to the pitch of the microlens grid. To evaluate its impact, just consider the simple case of the analysis of a null phase with an ordinary SHWFS (*H* small). Assuming a focal plane array with a fill factor of 1, the measured irradiance pattern $I_{NG}^m(x,y)$ is equal to

$$I_{NG}^m = \left(I_{NG}(x,y) * \Pi_{pix,pix}(x,y) \right) \text{comb}_{pix,pix}(x,y) \tag{38}$$

with pix being the pixel size. So, FTI_{NG}^m, the Fourier transform of the measured Hartmanngram is

$$FTI_{NG}^m(u,v) = \left(\Gamma_{\mu l}(u,v) \frac{\sin(\pi pu)}{\pi pu} \frac{\sin(\pi pv)}{\pi pv} \text{comb}_{1/p,1/p} \right) * \text{comb}_{1/pix,1/pix}. \tag{39}$$

The natural decrease in the amplitudes of the harmonics is thus amplified, due to the filtering of the pixel.

If we now consider the impact of the sampling step, we know that the farthest harmonic in the *u*-direction is placed at a spatial frequency f_{max}

$$f_{max} = \frac{2H_{NG}}{p} > \frac{2H}{p}. \tag{40}$$

So, we have to compare this frequency with the Nyquist frequency $f_{Nyq} = \frac{1}{2pix}$. Users ordinarily choose to place one spot on two pixels, so that

$$pix = \frac{\lambda f_{\mu l}}{p}. \tag{41}$$

Assuming this, we find that

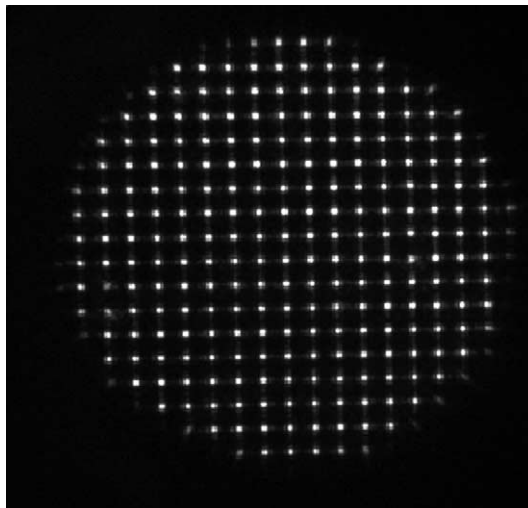$$\frac{f_{max}}{f_{Nyq}} > 2. \tag{42}$$

Fig. 6. Irradiance pattern recorded in the common focal plane of lenslets. SHWFS is made of 18 by 18 sub-apertures, with 12 by 12 pixels by sub-aperture. The microlens grid is rotated slightly to show the aliasing effects.
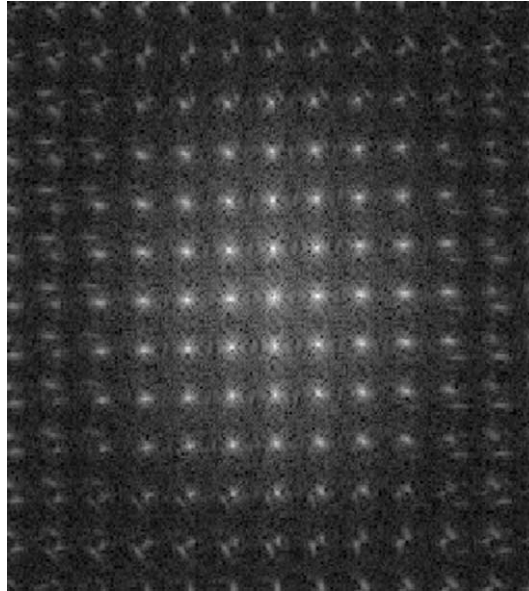
Fig. 7. Logarithm of the Hartmanngram spectrum. Notice the decrease of harmonics and the aliased harmonics, placed outside the square grid, at the edges of the figure. The progressive elongation of harmonics is due to aberrations.

So, the irradiance pattern is largely under-sampled, and highest harmonics are aliased onto lowest harmonics. However, due to their decrease, this effect is limited, especially for the first harmonics.

To illustrate this sampling problem, consider a SHWFS consisting of 18 sub-apertures across the diameter of the analyzed pupil. Each sub-aperture comprises 12 by 12 pixels, and the ideal focal spot (neglecting consecutive lenslets) is placed on 2 by 2 pixels, so H is equal to 6.

Fig. 6 shows the observed experimental Hartmanngram and Fig. 7, the logarithm of the modulus of its spectrum. The harmonics placed on a $1/p$ grid are clearly visible, with their decreasing amplitudes. The elongation of the more remote harmonics is due to aberrations, as the tested microlens array is of relatively poor quality. The microlens grid has been rotated slightly to show the aliasing. Thus, aliased harmonics appear as elongated spots, outside the square grid, at the edges of the figure.

4. Phase derivatives extraction

Another fundamental step for SHWFS is in the extraction of the phase derivatives. As described in the previous sections, one good way of obtaining this information for the two main directions x and y is to consider $\mathrm{Harm}_{1,0}(x,y)$ and $\mathrm{Harm}_{0,1}(x,y)$. However, most users prefer to estimate the phase derivatives by centroiding the local spots. The purpose of this paragraph is to demonstrate that these two processes are nearly the same.

Consider the centroiding operation in the x-direction, $\mathrm{Cenx}(x,y)$

$$\mathrm{Cenx}(x,y) = [I(x,y)\,\mathrm{Slope}(x)] * \Pi_{p,p}(x,y) \tag{43}$$

with I, the irradiance pattern, being equal to I_G or I_NG, and $\mathrm{Slope}(x)$ being the function presented in Fig. 8. The Fourier transform of $\mathrm{Slope}(x)$, $\mathrm{FTSlope}(u)$, is shown in Fig. 9. It is made of Dirac functions, with $1/x$ decreasing amplitudes. So, the Fourier transform of $\mathrm{Cenx}(x,y)$, $\mathrm{FTCenx}(u,v)$, is
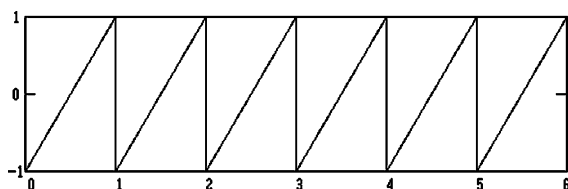
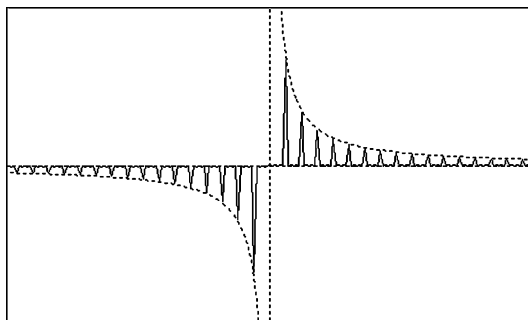Fig. 8. Slope(x), weighting function for centroiding evaluation (six sub-apertures).

Fig. 9. TFSlope(u), Fourier transform of Slope(x), for six sub-apertures. Dotted curve corresponds to $1/x$ function.

$$\text{FTCenx}(u,v) = \left(\sum_{k,l=-2H_{\text{NG}}}^{H_{\text{NG}}} \left[\text{FTHarm}_{k,l}^{\text{NG}} \ast \sum_{\substack{j=-\infty \\ j \neq 0}}^{+\infty} \frac{1}{j} \delta\left(u - \frac{k+j}{p}, v - \frac{l}{p}\right) \right] \right) \frac{\sin(\pi p u)}{\pi p u} \frac{\sin(\pi p v)}{\pi p v}, \qquad (44)$$

as $\sin(\pi p u)/\pi p u$ is equal to zero for $u = n/p$, we obtain

$$\text{FTCenx}(u,v) = \sum_{j=-\infty}^{+\infty} \frac{1}{j} \text{FTHarm}_{j,0}^{\text{NG}}(x,y), \qquad (45)$$

so

$$\text{Cenx}(x,y) \propto \sum_{j=1}^{+\infty} \frac{1}{j} \text{Im}\left(\text{Harm}_{j,0}^{\text{NG}}(x,y) \right). \qquad (46)$$

We have a weighted sum with decreasing weights of harmonics with decreasing amplitudes. So, for small H, we can say that the centroiding operation and the extraction of the imaginary part of $\text{Harm}_{1,0}^{\text{NG}}(x,y)$ are two nearly equivalent operations.
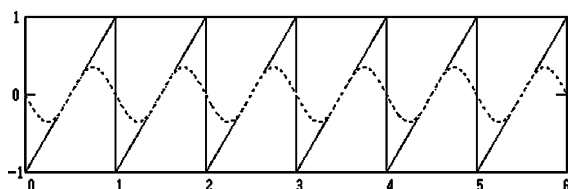

Fig. 10. Recommended sinusoidal function, for phase derivative extraction.

Moreover, it seems that the second technique is probably more precise because it is based on the harmonic which is almost unaffected by aliasing problems. In practice, the extraction of the imaginary part of the first harmonic is similar to the classical centroiding technique, just replacing the Slope(x) function by an appropriated sinusoid (see Fig. 10).

5. Conclusion

In this paper, we have demonstrated that the classical model used to describe the properties of SHWFS is not relevant for most applications. Indeed, the assumption of independent lenslets is not valid for most part of the applications, as it implies a compression ratio (ratio between the pitch and the size of the focal spot) greater than 20. For more appropriated compression ratio (from 2 to 8), the quantity measured by centroiding algorithm is proportional to the local phase derivative multiplied by a weighting function, depending on the compression ratio. The overall form of this weighting function shows that the high orders diffracted by the microlens array have no significant contribution. On the other hand, it differs significantly from the weighting function predicted by the classical model.

Considering the spectral analysis of the Hartmanngram, we have shown that the classical centroiding algorithm can be upgraded by replacing the periodical slope function by a simple sinusoid. This reduces the aliasing effects, existing in most applications, as only the first harmonic is taken into account.

To conclude, the model proposed here allows a better understanding of the SHWFS. It demonstrates that the way this measurement device acts on the analyzed wave-front is not so simple. Moreover, with this description, the SHWFS can be included in the large family of grating interferometers. It gives a simple theoretical basis to compare with other wave-front sensors such as lateral shearing interferometers [7–9]. We hope that the formulas detailed in the text will help in applications such as deconvolution from wave-front sensing or adaptive optics control, allowing a better description of the measured quantity.

References

[1] We have found more than 80 papers including ''Shack–Hartmann'' in the header using NEC Researchindex. A great majority is related to astronomy, and deals with adaptive optics control. These last years, ophtalmology is the emerging subject.
[2] Theoretical descriptions of Shack–Hartmann are found at the beginning of the above referenced papers. They are always based on the model originally proposed by Shack, in which lenslets are considered independently.
[3] R.V. Shack, B.C. Platt, J. Opt. Soc. Am. 61 (1971) 656.
[4] B.C. Platt, R. Shack, J. Refract. Surg. 17 (2001) September/October.
[5] F. Roddier, Opt. Eng. 29 (1990) 1239.
[6] J. Primot et al., J. Opt. Soc. Am. 7 (9) (1990) 1598.
[7] J.C. Wyant, Appl. Opt. 13 (1974) 200.
[8] C.L. Koliopoulos, Appl. Opt. 19 (1980) 1523.
[9] J. Primot, L. Sogno, J. Opt. Soc. Am. A 12 (12) (1995) 2679.